How to Cite:
Alibeigi, E., & Riazi, Z. Quantitative and qualitative evaluation of density resolution of pCT images using Cirs062m phantom simulation in Geant4. *International Journal of Health Sciences*, 5894-5909. Retrieved from https://sciencescholar.us/journal/index.php/ijhs/article/view/13401

Quantitative and qualitative evaluation of density resolution of pCT images using Cirs062m phantom simulation in Geant4

Ehsan Alibeigi
Physics and Accelerator Research School, Nuclear Science and Technology Research Institute, AEOI, P.O.Box: 14155-1339, Tehran – Iran.

Zafar Riazi*
Physics and Accelerator Research School, Nuclear Science and Technology Research Institute, AEOI, P.O.Box: 14155-1339, Tehran – Iran.

***Abstract*---**Accuracy in the treatment planning (TP) of proton therapy (PT) depends on the precision of the information employed to calculate the relative stopping power (RSP) of the tissues in the patient's body. This information is obtained from the x-ray computed tomography (xCT) images and the calibration curve needed to convert the Hounsfield unit to RSP values. Using xCT bears errors in proton range estimation and dose calculation of TP. Proton computed tomography (pCT) can decrease the inherent uncertainty in PT by directly measuring RSP. Though by using pCT in the integral mode of energy loss, this error is removed, and the RSP map of tissues is calculated directly. This study simulated a modern pCT imaging system with particle-by-particle tracking capability using Geant4 Monte Carlo code. This simulation sought to improve the density resolution of tissue images without increasing the dose. The CIRS062M standard phantom was irradiated with 300 MeV protons, and the energy, position, and direction of the particle were recorded before and after the phantom. The matrix of the RSP image was modified using the normalization algorithm of the amount of integral energy loss and the correction of the angles of the projections. The phantom image matrix was reconstructed as a RSP map using the filtered back projection (FBP) method. The results were compared in terms of dose, density resolution and root mean square error (RMSE) concerning real phantom image data. The proposed algorithm improved the density resolution from 9.1% to 4.3% and RMSE from 26.43% to 6.18% by correcting the angles of the projections at the same dose level.

***Keywords*---**Proton CT, FBP algorithms, Geant4, Cirs062M, Density Resolution.

Manuscript submitted: 9 May 2022, Manuscript revised: 18 July 2022, Accepted for publication: 27 August 2022

Introduction

PT is a precise external beam radiation therapy that uses high-energy protons to destroy cancerous tissues. This method Compared to conventional x-ray and electron treatment methods, creates higher doses in the target area, leading to improved treatment results for some types of cancer and reduced side effects [1-4]. In addition, due to the increasing awareness of the benefits of using charged particles, the PT centers are expanded worldwide [5-7]. In recent years, it has been estimated that more than 200,000 patients have been treated with a beam of charged particles [8-10]. On the other hand, reducing the error of RSP calculations is necessary to fully enjoy the benefits of PT, mainly related to proton range estimation and dose calculations for TP. Accuracy in the TP of PT depends on the accuracy of the information used to calculate the RSP of the tissues in the patient's body. The information related to the anatomy of the treated tissues and their electron density is obtained from xCT images and the calibration curve required to convert the Hounsfield unit to RSP values [11-15]. Conversion of electron density to RSP using the stoichiometric calibration method is the most widely used TP in PT centers worldwide. Since protons and photons are transmitted differently in the patient's body, additional and significant sources of error are created [16]. This conversion is a significant source of proton range calculation uncertainties, typically on the order of 3-5% of the proton range in TP [17].

By replacing the TP using pCT as a particle-by-particle tracking in the integral mode of energy loss, these errors are largely eliminated, and the RSP map of the tissues is calculated directly. pCT by directly calculating the RSP map in the patient despite the elimination of the position change caused by moving and transferring, remove the complications of using calibration curves to determine the RSP and reduce the received dose in determining the density resolution contrast. This method can reduce the uncertainty from 3 to 10 mm to 1 to 3 mm [15-18]. Figure (1) shows the effect of the error in radiation therapy with photon and proton [17].

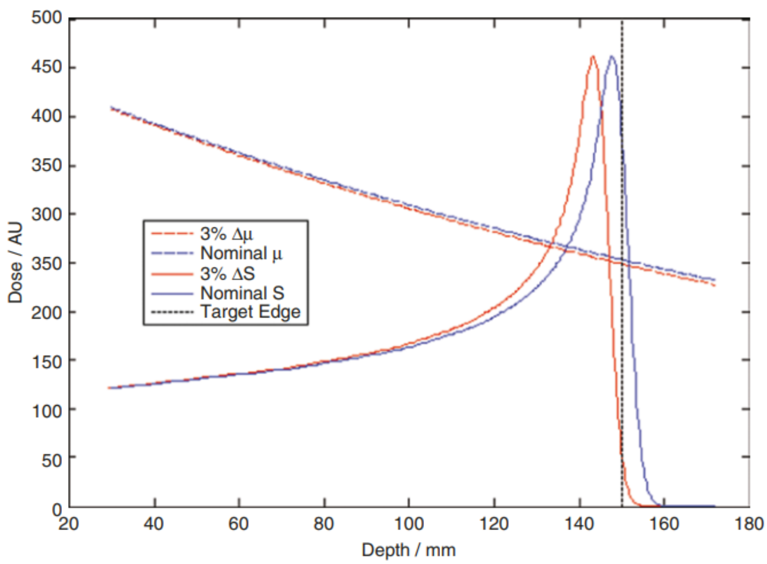

Figure 1. Comparison of the effect of a 3% increase in photon attenuation and proton stopping power on the applied field for radiotherapy [17]

The conducted studies indicate that the lack of attention to the safety margin of the range of charged particles can shift the location and the drop of the Bragg peak. As a result, the tumor dose will decrease, and the dose of healthy tissues will increase [19]. Different safety margins are provided in different proton therapy centers. For example, at Massachusetts General Hospital (MGH), the uncertainty in the proton beam range is assumed to be 3.5% plus an additional 1 mm [15].

Despite the advantages that pCT has, the physical phenomenon of multiple Coulomb scattering (MCS) derived from the random path of passing particles inside the material (small angle deviations by the Coulomb field of the nucleus) influences its spatial resolution. Since the early 1990s, due to advances in accelerator technology, position sensitive detectors, image reconstruction software and increasing interest in proton therapy have set new dimensions of studies to improve pCT for treatment planning use. This method is currently in the pre-clinical development stage and has become a research area of medical imaging [11, 15, 20].

This study modeled a modern proton computed tomography imaging system with particle-by-particle tracking capability. RSP values were calculated for a set of tissues inside the CIRS062M standard phantom. To this end, the excellent capabilities of Geant4 were used in the discussions of hadronic interactions and the selection of various models of electromagnetic interactions of particles with matter. The values of energy, position and movement direction of particle before and after the phantom were stored in a root file with 360 projections by rotating the phantom in one-degree steps. Then the integral energy loss in the phantom is obtained to calculate the relative stopping power of tissues. Radon transform is an Analytic reconstruction algorithm that was used to reconstruct the RSP sinogram matrix image. The resulting images were analyzed in dose, density resolution, and RMSE.

2. Proton Computed Tomography

As protons pass through matter, they lose most of their energy through inelastic collisions with outer atomic electrons. This leads to ionization and excitation. In addition, they are distorted by multiple small-angle scattering from the nuclei of the target material (multiple Coulomb scattering (MCS)). These two main processes, which happen many times along the macroscopic path of the proton, randomly lead to energy loss and deviation from the main direction of the proton beam [21-24]. With these interpretations, the proton imaging system can be performed in three ways depending on the type of interaction with matter: 1) attenuation, 2) nuclear scattering, and 3) energy loss. In this respect, Koehler et al. showed in 1968 that proton beam attenuation compared to X-ray produces images with better contrast and lower dose but poor spatial resolution [25]. In this regard, Hanson et al. established in 1979 that by measuring the energy loss of protons, the spatial resolution of images can be improved. As a result, they presented the design of proton computed tomography in 1981 with the method of measuring the residual energy in the collection of projections necessary to form the image [11-12].

The basis of the imaging function is the energy loss method to study the changes in the energy of the proton passing through the target as normative measures of its electron density. The energy loss of protons that pass through an object is related to the integral of the path. This relationship can be used to reconstruct the electron density distribution. A similar relationship is used to measure x-ray attenuation - with the difference that x-rays travel straight to the detector, but protons travel a curved path due to MCS [22- 24].

Since the amount of energy loss by the passage of protons through the medium (RSP of the tissue) depends on the energy of the proton and the chemical composition of the material, the result of imaging is a map of the RSP of the tissue. The average rate of proton energy loss is obtained through equation (1), known as Bethe-Bloch.

$$\frac{dE}{dx}(x) = \eta_e S(I(r), E(r)) \tag{1}$$

$$S(I(r), E(r)) = k\frac{1}{\beta^2(E)}\left[\ln\left(\frac{2m_e c^2}{I(r)}\frac{\beta^2(E)}{1-\beta^2(E)}\right) - \beta^2(E)\right]$$

In equation (1), r is the location, η_e is the relative electron density, I(r) is the mean excitation energy (I-value), S(I(r), E(r)) is the stopping power function, and E(r) is the proton energy at the point r. The changes in the I-value are relatively small, and the dependence of the S function on I is relatively low due to the logarithmic nature of the changes [26-27]. RSP is rewritten as equation (2) by integrating the relative electron density.

$$\int_S \eta_e(r)dx = \int_{E_{out}}^{E_{in}} \frac{dE}{S(I_{water}, E)} \tag{2}$$

In relation (2), having the I-value for water (75eV) and measuring the values of input energy (E_{in}) and output energy (E_{out}), the integral on the right side of relation (2) can be calculated numerically. As a result, particle-by-particle proton tracking detectors are used to reconstruct proton images. Figure (2) schematically shows the computer tomography of a proton with particle-by-particle tracking capability. To measure the RSP value of the tissues, the detectors obtained by exposing the phantom to radiation are used. A beam of protons with a specific energy E emits on the considered phantom and leads to the loss of part of the initial energy inside the phantom.

Four sets of position-sensitive detectors (PSD) record the position and direction of particles before and after the phantom: PSD 1, PSD2, PSD3, and PSD4. And the amount of energy loss (ΔE) inside the sample is estimated from the measurement of the residual energy range detector (RERD). Using these recorded data, the integral of the relative electron density of the material along the path of a proton inside the phantom is acquired from equation (2) [12].

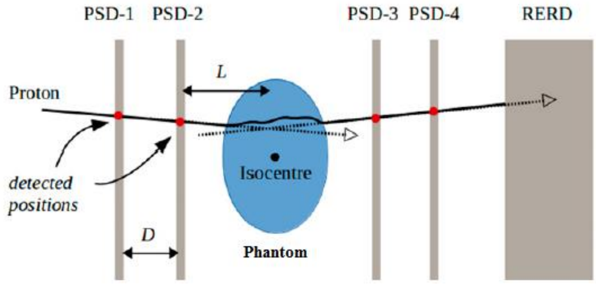

Figure 2. Comprehensive design of proton computed tomography using energy loss method with PSDs and RERD [12].

3. Simulation

Modeling pCT imaging system in Geant4 code

Geant4 code is a powerful software for simulating fundamental particle interactions and is written in C++ programming language. This software is employed for studies in high-energy physics, nuclear physics, astronomy, medicine, and basic studies in ionizing radiation. One of the most critical benefits of this simulation code is the wide range of energy, the Physics of the Universe, and the number of different particles. In hadronic topics, the physics list QGSP_BIC_EMY is used to improve the accuracy of the simulation. This list provides QGSP hadronic models for nucleons, BIC inelastic models for ions, and EMY electromagnetic models for all particles.

The simulation includes geometry selection, physic lists, and primary generation and output parameters. The studied geometry includes the CIRS062M phantom, the beamline from the accelerator to the phantom, the particle-to-particle tracking system before and after the phantom (PSD detectors), and the residual energy range detector. The geometry design generally contains the shape and selection of the materials used, and the Geant4 code based on these materials forms the cross-sectional table of interactions at the start of the program execution.

The CIRS062M standard phantom consists of a disk with a diameter of 33 cm and a height of 5 cm, the surrounding material of which is water-equivalent plastic, and 16 small disks inside with a diameter of 2.6 cm from different materials listed in Table (1) [28].

Table 1. Information about the elements used in the simulated phantom [28]

Insert Material	Name	Relative electron density	Relative stopping power
Lung(Inhale)	Lu(I)	0.195	0.215
Lung(Exhale)	Lu(E)	0.51	0.482
Breast	Brst	0.991	0.991
Trabecular Bone	B200	1.161	1.091
Liver	Liv	1.072	1.058
Muscle	Msc	1.062	1.043

Adipose	Adi	0.967	0.967
Dense Bone	B800	1.53	1/402
Cortical Bone	B1250	1.83	1/616
Water plastic	Water plastic	1/029	1/005

The position-sensitive detectors 2 and 3 were considered at a distance of 1 centimeter before and after the phantom. And the distance of the source used for simulation in the form of 300 MeV single-energy protons was chosen 5 cm from the beginning of the phantom and was randomly emitted at the phantom in the height range of -20 to 20 cm. By rotating the phantom 360 degrees with 1-degree steps, the detectors recorded the location (x, y, z), the angle of entering and leaving the phantom, and the residual energy of each proton. They saved it in the output file of the root software.

Next, the integral on the right side of relation (2) was calculated in MATLAB software, and the resulting projections were stored in the sinogram matrix with 360×400 dimensions. Using the image reconstruction algorithms applied to the data, the density resolution of the images acquired from the standard phantom was checked. Figure (3) displays an image of the designed components in the pCT with the Geant4 Monte Carlo code and the time when 1000 proton particles were emitted at the phantom. This figure demonstrates the path of movement and interaction of protons with the phantom in the residual energy detector. The

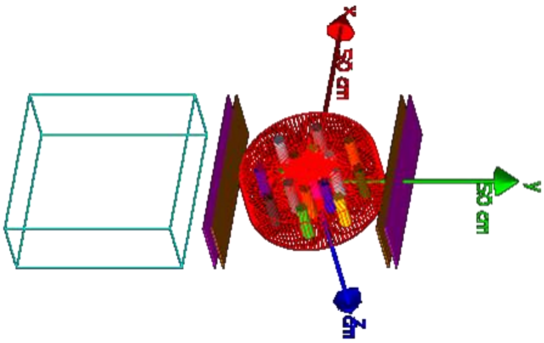

profile of changes in energy deposition in the remaining detector shows the changes of RSP in the path of movement.

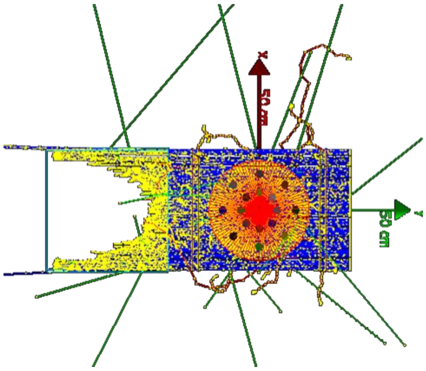

Figure 3. pCT modeling of energy loss with particle-by-particle tracking capability in Geant4 code.

4. Image reconstruction

The image projections information in pCT consists of the integral energy loss of proton along the path between the source and the detectors. The image is obtained by processing the projections from the object at different angles. If the common FBP analytical reconstruction approach based on direct problem solving is used to reconstruct the pCT data, the proton movement path is considered a straight line. Proton deflection because of MCS makes its movement path inside the material out of the straight line, which weakens the spatial resolution of the resulting images. Different Monte Carlo studies have indicated that employing FBP for temporal reconstruction is suitable as the first assessment of the target during the pre-treatment patient positioning process [29].

For improved the quality of proton images in reconstruction algorithms, proton trajectory tracking is used, which estimate the Most Likely Path (MLP) of the proton with hardware facilities (PSD). In this technique, information about each pixel of the detector is available to enhance the quality of the reconstructed images. Although MLP is the best path estimation among the studied cases, it is mathematically complex and computationally costly. Analytical algorithms based on Radon transform optimize image reconstruction when the number of collected projection is large [30-32].

This research uses an analytical method based on Radon transformation for image reconstruction. The first mode considered for image reconstruction is employing the FBP algorithm. In this case, the amount of proton energy loss at each angle is calculated and attributed to the total energy loss of the pixels of the proton path. This approach considers the same contribution for each pixel along the path acquired by directly solving problem of sinogram for integral energy loss of proton path. Hann filter is employed to decrease blurring and increase the quality of the resulting image.

In the second mode, considering that the number of protons passing through the material is different in various parts of the phantom, it is essential to normalize the integral energy loss obtained in each pixel concerning the number of particles passing through that pixel. Since detectors sensitive to the particle position are used for tracking in pCT design, the information available in each pixel of the detectors during entry and exit from the phantom for 100,000 primary emitting particles is available in the output. According to this information, the modified integral energy loss enhances the image quality. So that in each path, the integral energy loss was divided by the number of particles passing through each detector pixel, and the modified sinogram was obtained and reconstructed using the FBP algorithm.

In the third mode, according to MCS, applying angular corrections to the modified sinogram and FBP algorithm are used to decrease the error. In this mode, the slope of the proton trajectory angle between the entry and exit point is calculated, and the conditions for correcting the angle of incidence in the modified sinogram are considered. If the slope of the angle obtained from the single projections in the θ angle includes one of the following conditions, the resulting single projections is removed from the θ angle projections and added to its corresponding angle projections.

$1 \leq \theta$
$\theta \geq -1$
$-1 \leq \theta \leq 1$

5. Results

The results of 300 MeV pCT simulations for the CIRS phantom model 062M were stored in the integral energy loss mode using root software in Geant4 code. Figures (4) and (5) shows the normalized integral energy loss of profile for 100,000 initial emitting particles at 0 and 90 degrees, respectively.

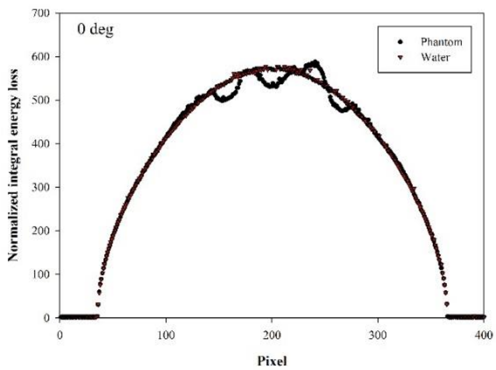

Figure 4. Projections profile of the normalized integral energy loss at 0°

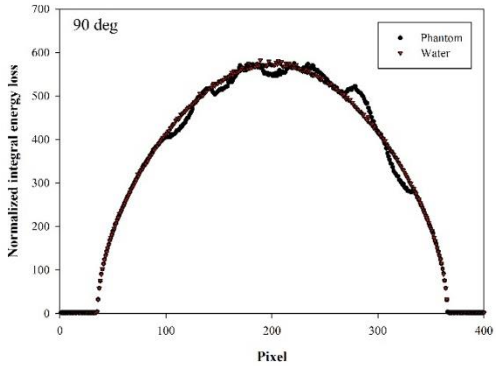

Figure 5. Projections profile of the normalized integral energy loss at 90°

To check the changes in the projection profiles of the resulting tissue-equivalent disks inside the phantom, in figures (4) and (5), the profile of the projection from the environment (plastic equivalent to water) was also calculated.

Comparing these two figures (4) and (5) proves that the profiles of 0 and 90-degree projection change due to the change of material density along the proton path by changing the angle. This demonstrates the sensitivity of the pCT method in the integral energy loss mode to the density changes created along the phantom rotation. To better examine the performance of pCT, 11 response lines are shown in Figure (6): lines 1, 2, 3, 4, 5, and 6 for the resulting 90-degree projections profile, and lines 7, 8, 9, and 10. and 11 for the 0-degree projections profile.

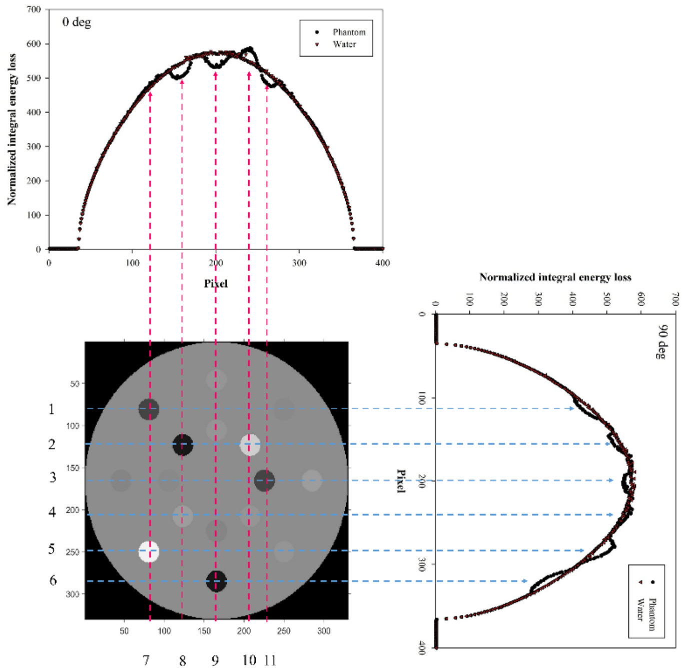

Figure 6. The effect of Superposition principle tissues with different RSP on the integral energy loss projections profile at 0 and 90 degree

As it is seen, in the location of bone tissues (such as response lines 5 and 10), integral energy loss of protons increases because of the greater RSP of bone compared to water plastic. This phenomenon causes a bump in the profile of the projections. Also, in the location of softer tissues (such as response lines 6 and 11), the integral energy loss of protons decreases due to the smaller RSP compared to water plastic. This reduction emerges as a recess in the profile of the projections. It is possible for protons to alternately pass through tissues with different RSPs during their path. The integral energy loss profile will display the effect of Superposition principle disks in Cirs062M phantom with different RSPs. Response line 7 in Figure (6) includes a bone disk and a lung (Exhale) disk, which neutralize each other's effect in the projections profile. And their collective effect is nearly equivalent to water plastic. For a better grasp of this impact, by referring to Table (1), it can be seen that the total RSP of disks along the route of line 7 divided by the number of disks is 1.049, emerging as a very tiny bump in the projections profile of the integral energy loss (response line 7).

The projection acquired from the results of RSP phantom solution along the proton path was converted into an image matrix with dimensions 360×400. By extracting the image characteristic of each tissue from the image matrix, the RSP map of the standard phantom material was revealed in pCT. To check the density resolution of reconstructed images, the studied phantom was simulated in MATLAB software with the data in Table (1). Figure (7) shows the combination of elements used in the phantom.

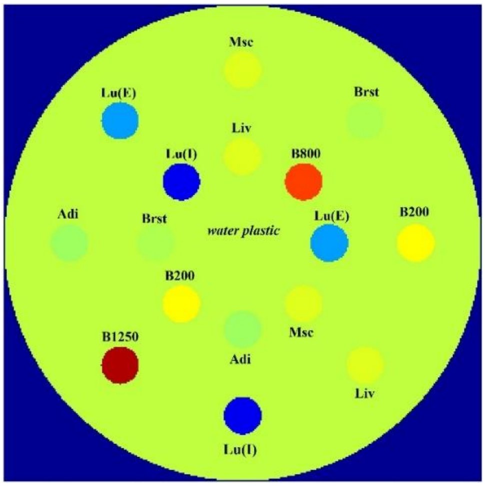

Figure 7. CIRS 062M phantom image of the combination of elements used in Geant4 code simulation

Figure (8) shows the cross-sectional image resulting from the reconstruction of the information integral energy loss with the FBP algorithm for the CIRS062M phantom. In Figure (8), Lu(I), Lu(E), B200, B800, and B1250 tissues are separated from the background environment (water plastic). On the other hand, since Msc, Liv, Brst, and Adi tissues cannot be distinguished from the background, the density resolution obtained in this image is 9.1%. As it is clear from Figure (8), the signal-to-noise ratio in the image is low.

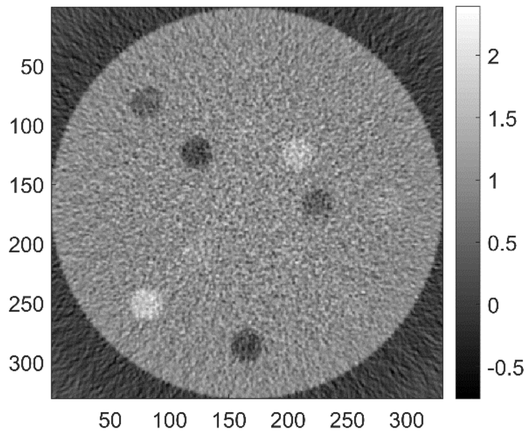

Figure 8. cross-sectional image of integral energy loss projections with FBP from cirs062M phantom

Enhancing the quality of CT images to reduce the error in the treatment planning of proton therapy has always been one of the most critical and most challenging parts of image processing. For accurate interpretation and decision-making, the presence of high-quality images is vital. One of the suggested solutions to improve the signal-to-noise ratio by increasing the dose. Figure (9) shows the image resulting from the reconstruction of the integral energy loss data with a twenty-fold increase in dose. As a result of this increase, the number of visible disks in the standard phantom increases, so the only tissue-equivalent disks not seen in the image are Adi and Brst. In this mode, the accuracy in density resolution to 4.3% with increasing dose.

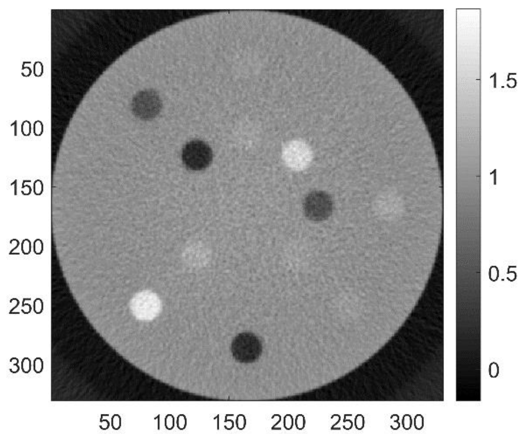

Figure 9. cross-sectional image of integral energy loss projections from dose increase with FBP

The initial design of pCT was based on energy loss and detectors sensitive to the position of the particle were used. as a result, the information available in each pixel during entry and exit from the phantom for 100,000 primary particles in the output file. According to the relevant information, algorithms were written to enhance the quality of images. Figure (10) indicates the image resulting from the reconstruction of the standard phantom image for 100,000 primary incident particles by applying the FBP algorithm and operating the modified sinogram with the number of protons. The results show an improved signal-to-noise ratio, and a density resolution of 4.3% was obtained, equaling the density resolution of figure 9 at 20 times the dose.

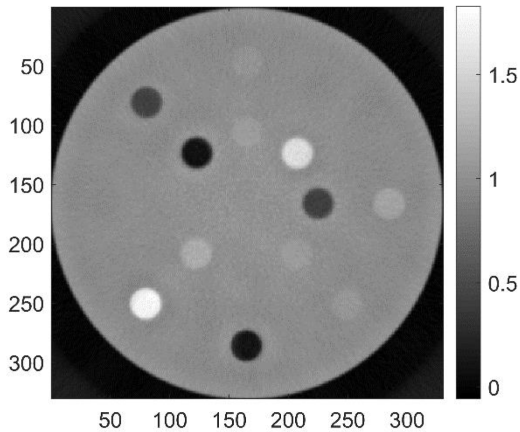

Figure 10. cross-sectional image of integral energy loss projections with modified sonogram by number of proton in pixel

The quality of pCT images is limited because of the random nature of the proton passage inside the object. Multiple tiny angle scattering caused by the nuclear Coulomb field of the nucleus causes the exact path of the proton to be accompanied by deviations. Hence, the reconstruction of the images acquired from measuring the amount of integral energy loss of protons concerning these deviations leads to decreased spatial resolution. Figure (11) is the image resulting from the reconstruction of the standard phantom image for 100,000 initial emitting particles with the correction of the number of projections based on the angle according to the three conditions of the angle corrections in the sinogram modified with the FBP algorithm. In this mode, 16.7% of the projections were transferred to the projections corresponding to their angle by correcting the angle. The results of this angle correction led to the improvement of the total image error compared to the image of the standard phantom.

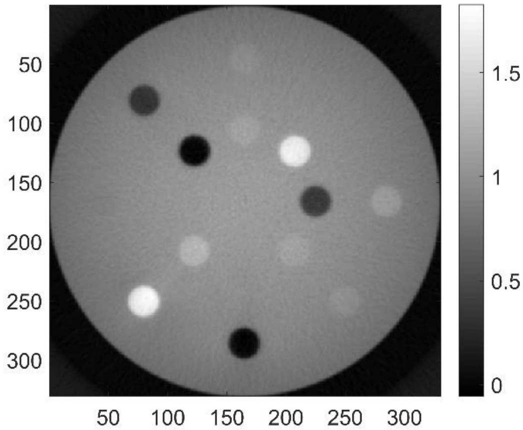

Figure 11. cross-sectional image of integral energy loss projections with modified sonogram by number of proton in pixel and correcting angel

For checking the root mean square error (RSME) of each technique, the pixel intensity value of the phantom images was compared with the actual real phantom data image in MATLAB software. Equation (3) demonstrates how to calculate RSME:

$$RSME = \sqrt{\sum_{i,j=1}^{n} \frac{(Image_{i,j} - Phantom_{i,j})^2}{n}} \tag{3}$$

The results of different methods are compared in Table (2).

Table 2. Comparison of the results of applied reconstruction methods

Image reconstruction method	RMSE*	Number of disk seen in the image	Minimum RSP of disk seen in the image	Number of proton emitted
FBP	23.43	8	1.091	10^5
FBP	8.82	12	1.043	2×10^6
FBP with corrected sinogram	6.93	12	1.043	10^5
FBP with corrected sinogram and angle	6.18	12	1.043	10^5

* Root Mean Square Error

6. Discussion and Conclusion

Presently, tissue density maps in the TP of PT are obtained through xCT images and using calibration curves, which is associated with an error of 3% in estimating the proton range. Another drawback of converting the Hounsfield unit to RSP is its deficiency in identifying materials with the same density but different elemental compositions of tissues caused by the photon interaction mechanism. This issue is critical in the targeted TP at the borders of two tissues with identical densities. pCT has two important advantages in medical applications: (1) using this method as an ideal and online method for calculating directly obtaining three-dimensional RSP maps, which leads to reducing the error; and (2) its dose for image reconstruction is significantly lower than xCT for a given same density resolution. The extensive capabilities of these systems in reducing the uncertainties in calculating the RSP values of tissues and the primary energy of incident protons have caused the increasing attention of scientific centers to improve the accuracy and precision of pCT.

In the general, the quality of pCT images is limited by range straggling, MCS and Inelastic nuclear interactions. The purpose is to enhance the fundamental factors in proton imaging, namely spatial resolution, density resolution, and imaging dose. These contain accurate data selection and reliable and fast reconstruction algorithms processing. Considering the complicated nature of the interaction of charged particles, treatment planning using these particles needs different approaches in data processing and image reconstruction compared to xCT.

One of the cases examined in this study is the function of dose increase in reducing noise and increasing the number of visible tissues. The relevant results are listed in Table (2). The error of the images increases owing to the decline of the count per pixel and its noise. To overcome the error, the number of particles can be increased. This requires a longer simulation time. Furthermore, according to the technique used based on the particle by particle tracking, the amount of information is greater, and data processing becomes heavier and more time-consuming.

Another thing investigated is to take advantage of the pCT tracking system using existing detection technologies. In this research, the impact of normalizing the amount of integral energy loss is calculated by the number of protons passing through each pixel. This method was employed in FBP image reconstruction. The results indicated that the modified sinogram yields an improved quality of the images. In this method, the intensity difference of adjacent pixels is decreased, the contrast of the resulting images is reduced, and it is not considered suitable in phantoms where the materials used in them have electron density close to each other.

In the pCT with particle-by-particle tracking, position, direction and energy information of each proton is recorded. To this end, to enhance the quality of the image at a lower dose, this capability was employed by acquiring the proton intensity sinogram to lower the noise applied to the images. Furthermore, reducing the amount of MCS applied in the modified sinogram reduced the error of using the algorithm for image reconstruction. The compared results that if the

FBP algorithm is used with a modified sinogram and angle corrections are applied at a lower dose, the signal-to-noise ratio is increased, and the RMSE is reduced 2.64%.

References

1. *Wong, C. J., et al., High-resolution measurements of small field beams using polymer gels, Applied Radiation and Isotopes. 65.10, 1160-1164 (2007).*
2. *Khan, Faiz M., and Bruce John Gerbi, Treatment planning in radiation oncology, Wolters Kluwer Health/Lippincott Williams & Wilkins. (2012).*
3. *Levin, W. P., Kooy, H., Loeffler, J. S., Laney, T. F., Proton beam therapy, British J Cancer. 93, 849–854 (2005).*
4. *4. Attanasi, F. et al., Experimental Validation of the Filtering Approach for Dose Monitoring in Proton Therapy at Low Energy, Phys Med. 24, 102–106 (2008).*
5. *Almehmadi M, Alzahrani K, Salih MM, Alsharif A, Alsiwiehri N, Shafie A, Almalki AA, Dahlawi H, Al-hazmi A, Al-Khalidi A, Al-ghoraibi N. Assessment of thyroid gland function by evaluating of TSH, FT3 and FT4 hormones in untreated cancer patients. J. Adv. Pharm. Educ. Res. 10(4): 37-42 (2020).*
6. *Alhomayani FK, Althumali AM, Alhamyani A, Alsufyani AA, Alharthi NA, Almalki MS. Awareness of hemodialysis patients regarding symptoms of cancer at king Abdul-Aziz specialized hospital, Taif city. Arch. Pharm. Pract. Apr 1;11(2): 69-80 (2020).*
7. *Alhuzaim W, Alosaimi M, Almesfer AM, Al Shahrani NM, Alali AH, Alibrahim KI, Beayari SM, Bugshan TF, Kamal AJ, Almuraydhi KM, Almukhaitah AA. Saudi Patients' Knowledge, Behavior, Beliefs, Self-Efficacy, and Barriers Regarding Colorectal Cancer Screening. Int. J. Pharm. Res. Allied Sci. Jan 1;9(1): 14-20 (2020).*
8. *Jakel, O, State of the art in hadron therapy, AIP Conference Proceedings. 95, 70-77 (2007).*
9. *K.W.D.Ledingham, P.R.Bolton, N.Shikazono, C-M.Ma, Towards Laser Driven Hadron Cancer Radiotherapy, A Review of Progress. Med Phys. (2014).*
10. *https://www.ptcog.ch.*
11. *M. Prall et al. High-energy proton imaging for biomedical applications, scientific reports 6. 27651 (2016).*
12. *G. Poludniowski, N.M. Allinson, and P.M. Evans. Proton radiography and tomography with application to proton therapy, The British journal of radiology. 88.1053, (2015).*
13. *Li, Tianfang, et al. Reconstruction for proton computed tomography by tracing proton trajectories: A Monte Carlo study, Medical physics 33.3 (2006).*
14. *M. Bucciantonio, and F. Sauli. Proton computed tomography, Modern Physics Letters A. 30.17, (2015).*
15. *M. Yang et al. Comprehensive analysis of proton range uncertainties related to patient stopping power- ratio estimation using the stoichiometric calibration, Physics in Medicine and Biology. 57.13, 4095–4115 (2012).*
16. *C. Zeng et al. Proton Treatment Planning, Target Volume Delineation and Treatment Planning for Particle Therapy. Springer, Cham. 45-105 (2018).*
17. *Bucciantonio, Martina, and Fabio Sauli, Proton computed tomography, Modern Physics Letters A. 30.17, (2015).*
18. *Zeng, Chuan, et al, Proton Treatment Planning, Target Volume Delineation and Treatment Planning for Particle Therapy. Springer, Cham. 45-105 (2018).*

19. *Paganetti H, Range uncertainties in proton therapy and the role of Monte Carlo simulations, Physics in Medicine and Biology. 57.11,99 (2012).*
20. *Quinones, Catherine Thérèse, Proton computed tomography, Diss. Université de Lyon. (2016).*
21. *Schulte, Reinhard, et al. Conceptual design of a proton computed tomography system for applications in proton radiation therapy, IEEE Transactions on Nuclear Science 51.3 (2004).*
22. *Li, Tianfang, and Jerome Zhengrong Liang. Reconstruction with most likely trajectory for proton computed tomography, Medical Imaging 2004: Image Processing. Vol. 5370. International Society for Optics and Photonics, (2004).*
23. *Williams, David C. The most likely path of an energetic charged particle through a uniform medium, Physics in Medicine & Biology 49.13 (2004).*
24. *Schulte, R. W., et al. A maximum likelihood proton path formalism for application in proton computed tomography, Medical physics 35.11 (2008).*
25. *Koehler. Proton radiography, Science (New York, N.Y.). 3825, 303–304(1968).*
26. *Erdelyi, B. A comprehensive study of the most likely path formalism for proton-computed tomography, Physics in Medicine & Biology 54.20 (2009).*
27. *Li, T., et al., Reconstruction for proton computed tomography: a Monte Carlo study, IEEE Medical Imaging Conference. (2003).*
28. *Erich Schnell, Salahuddin Ahmad and Tania de la Fuente Herman, Commissioning of a Relative Stopping Power to Hounsfield Unit Calibration Curve for a Mevion Proton Radiation Treatment Unit, University of Oklahoma Health. (2016).*
29. *Quiñones, C. T., J. M. Létang, and S. Rit. Filtered back-projection reconstruction for attenuation proton CT along most likely paths, Physics in Medicine & Biology 61.9 (2016).*
30. *Khellaf, Feriel, et al. A comparison of direct reconstruction algorithms in proton computed tomography, Physics in Medicine & Biology 65.10 (2020).*
31. *Collins-Fekete, Charles-Antoine, et al. A theoretical framework to predict the most likely ion path in particle imaging, Physics in Medicine & Biology 62.5 (2017).*
32. *Rit, Simon, et al. Distance-driven binning for proton CT filtered back projection along most likely paths, Second International Conference on Image Formation in X-Ray Computed Tomography, Conference Paper. (2010).*